Alexandria Engineering Journal (2016) 55, 569–581

HOSTED BY

ELSEVIER

Alexandria University

Alexandria Engineering Journal

www.elsevier.com/locate/aej
www.sciencedirect.com

ORIGINAL ARTICLE

Heat and mass transfer effects on the mixed convective flow of chemically reacting nanofluid past a moving/stationary vertical plate

B. Mahanthesh [a,b], B.J. Gireesha [b,c,*], Rama Subba Reddy Gorla [c]

[a] *Department of Mathematics, AIMS Institute of Higher Education, Peenya, Bangalore 58, Karnataka, India*
[b] *Department of Studies and Research in Mathematics, Kuvempu University, Shankaraghatta-577 451, Shimoga, Karnataka, India*
[c] *Department of Mechanical Engineering, Cleveland State University, Cleveland 44114, OH, USA*

Received 4 July 2015; revised 21 January 2016; accepted 27 January 2016
Available online 12 February 2016

KEYWORDS

Nanofluid;
Heat and mass transfer;
Thermal radiation;
Laplace transform technique;
Chemical reaction;
Nusselt and Sherwood number

Abstract The problem of conjugate effects of heat and mass transfer over a moving/stationary vertical plate has been studied under the influence of applied magnetic field, thermal radiation, internal heat generation/absorption and first order chemical reaction. The fluid is assumed to be electrically conducting water based Cu-nanofluid. The Tiwari and Das model is used to model the nanofluid, whereas Rosseland approximation is used for thermal radiation effect. Unified closed form solutions are obtained for the governing equations using Laplace transform method. The velocity, temperature and concentration profiles are expressed graphically for different flow pertinent parameters. The physical quantities of engineering interest such as skin friction, Nusselt number and Sherwood number are also computed. The obtained analytical solutions satisfy all imposed initial and boundary conditions and they can be reduced to known previous results in some limiting cases. It is found that, by varying nanoparticle volume fraction, the flow and heat transfer characteristics could be controlled.

1. Introduction

In many industrial and engineering applications, the heat and mass transfer is a consequence of buoyancy effects caused by thermal diffusion and chemical species. Therefore, the study of conjugate effects of heat and mass transfer is handy for improving many technologies such as underground energy transport, polymer and ceramics production, enhanced oil recovery, food processing, formation and dispersion of fog, the distribution of temperature and moisture over agricultural fields, and environmental pollution. The heat and mass

* Corresponding author at: Department of Mechanical Engineering, Cleveland State University, Cleveland 44114, OH, USA, Department of Studies and Research in Mathematics, Kuvempu University, Shankaraghatta-577 451, Shimoga, Karnataka, India.
E-mail addresses: bmanths@gmail.com (B. Mahanthesh), g.bijjanal-jayanna@csuohio.edu (B.J. Gireesha), r.gorla@csuohio.edu (R.S.R. Gorla).
Peer review under responsibility of Faculty of Engineering, Alexandria University.

http://dx.doi.org/10.1016/j.aej.2016.01.022
1110-0168

Nomenclature

$\boldsymbol{B}$	magnetic field
b	body forces
B_0	magnetic field strength
C	concentration of the fluid
C_f	skin friction co-efficient
c_p	specific heat coefficient of fluid (J/kg K)
D	mass diffusion co-efficient
$\boldsymbol{E}$	electric field
f	dimensionless velocity component
g	acceleration due to gravity
Grt	thermal Grashof number
Grc	solute Grashof number
$\boldsymbol{J}$	current density
j	mass flux
k^*	Rosseland mean absorption co-efficient
k	thermal conductivity (W/mK)
k_1	chemical reaction co-efficient
K	chemical reaction parameter
M^2	magnetic parameter
Nu	Nusselt number
Pr	Prandtl number
Q_0	uniform volumetric heat source/sink
Q	heat source/sink parameter
q	heat flux
q_r	radiative heat flux
R	thermal radiation parameter
Sc	Schmidt number
Sh	Sherwood number
t	time
T	fluid temperature (K)
u_0	constant
$u,\ v,\ w$	velocity components along x, y, and z directions ($\mathrm{m\ s^{-1}}$)
x	coordinate along the plate (m)
y	coordinate normal to the plate (m)

Greek symbols

∇p	pressure gradient
ν	kinematic viscosity ($\mathrm{m^2\ s^{-1}}$)
μ	dynamic viscosity ($\mathrm{kg\ m^{-1}\ s^{-1}}$) shear rate
ϕ	nanoparticle volume fraction
σ^*	Stefan–Boltzmann constant
σ	electrical conductivity
ρ	density ($\mathrm{kg/m^3}$)
β_T	thermal expansion co-efficient
β_c	solutal volumetric coefficient
λ	moving parameter
θ	dimensionless temperature
φ	dimensionless concentration
$\eta,\ \tau$	dimensionless variables

Subscripts

f	base fluid
nf	nanofluid
s	nanoparticles
w	at the wall condition
∞	far from the wall

Constants $x_1 - x_6, a_1 - a_9, b_1 - b_2, f_1 - f_7, g_1 - g_7$

transfer flow of an electrically conducting fluid in the presence of transverse magnetic field also finds a variety of applications such as MHD generators, pumps, flow meters, nuclear reactors, accelerators and in metallurgical industries. Its relevance is also seen in many practical applications in geophysical and astrophysical situations [1]. Sarpkaya [2] was the first to study the effectiveness of MHD flows in fluids. A few recent studies regarding MHD heat and mass transfer with different physical conditions are [3–12].

On the other hand, the radiative heat transfer has encountered a variety of applications such as nuclear power plants, gas turbines, and propulsion devices for space vehicles, missiles and aircraft. Additionally, heat and mass transfer under the influence of chemical reaction has also attracted considerable attention of many authors due to their wide range of applications. Keeping this in view, conjugate heat and mass transfer flow past a vertical permeable plate with thermal radiation and chemical reaction is investigated by Pal and Talukdar [13]. They found that, the thermal radiation and chemical reaction effect decrease the velocity and concentration profiles. Numerical investigation of heat and mass transfer of an electrically conducting fluid over a moving surface with first order chemical reaction effect is carried out by Chamkha [14]. Uwanta and Omokhuale [15] have analyzed the influence of radiation and chemical reaction effect on heat and mass transfer of a viscoelastic fluid in a fixed plane. Later, the combined effects of radiation and chemical reaction on the MHD free convection flow of an electronically conducting viscous fluid over an inclined plate have been studied by Ali et al. [16] and have obtained a closed form solution by employing Laplace transform technique. Das et al. [17] came up with an analytical solution for the problem of unsteady free convection flow and mass transfer over a vertically moving plate in the presence of thermal radiation using Laplace transform method. Several attempts have been made to analyze the effect of thermal radiation and chemical reaction under various physical situations (see [18–24]).

In recent times, the heat/mass transfer analysis in nanofluids has been the topic of extensive research due to intensification of thermal properties in heat transfer processes. The nanofluids can be described as a mixture of nanometer sized particles (diameter less than 100 nm) in the base fluid. The nanoparticles are prepared from copper, aluminum, titanium oxide, gold and the materials that are stable chemically. The base fluids are ordinary fluids, including water, toluene, ethylene glycol and mineral oils. In a wide variety of industrial and engineering applications, the transfer of heat energy is a common and necessary process, and the enrichment of heating/cooling in an industrial process may create a number of advantages such as energy saving, reduction of processing time and also the greater quality of the final product. However, the heat transfer efficiency also depends on the thermal

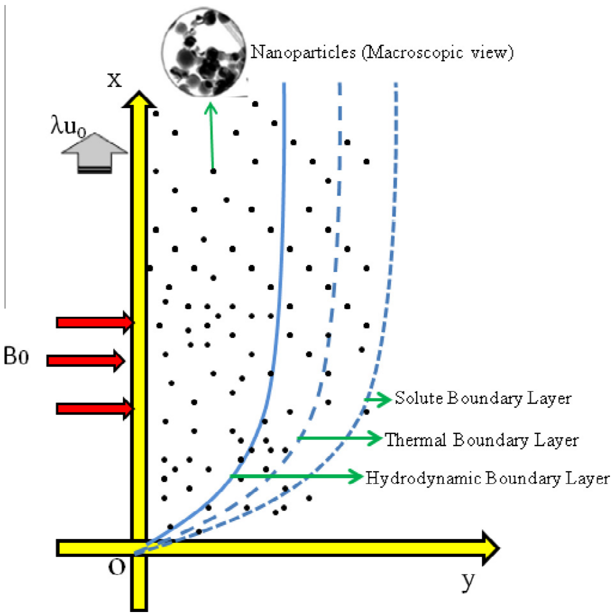

Fig. 1 Physical system and Geometry of the problem.

performance of working fluids. Thus, improving the thermal conductivity of working fluids becomes a major and challenging task for industrial necessity. The inspiration of suspended nanoparticles in a base fluid to increase the thermal conductivity was proposed by Choi [25] about a decade ago. Thereafter, theoretical and experimental investigations on the nanofluid heat transfer property have been conducted by Wang et al. [26], Eastman et al. [27], Buongiorno [28], etc. They have concluded that the thermal conductivity of the base fluid can be dramatically enhanced in the presence of nanoparticles. Besides, there are two models are available to incorporate nanoparticle effect on fluid flow problems namely single-phase model and two-phase model. Further, Buongiorno or Tiwari and Das model is used to model the single-phase nanofluid. Two important mechanisms such as Brownian motion and thermophoresis are treated in Buongiorno model. However, in Tiwari and Das model, the effective fluid properties are taken into account.

The nanofluids have tremendous applications such as engine cooling, solar water heating, cooling of electronic equipments, cooling of transformer oil, cooling of heat exchanging devices, in chillers, refrigerator–freezers, nuclear reactors, and space vehicles, due to their higher thermal conductivity and convective heat transfer rates. Recently, Sheikholeslami and Ganji [29] studied the MHD effects on nanofluid flow in a permeable channel. Kuznetsov and Nield [30] critically analyzed the natural convection flow of a nanofluid past a vertical plate. The problem of transient MHD free convection flow of a nanofluid over a rotating vertical plate is addressed by Hamad and Pop [31]. They solved the governing equations analytically using the perturbation method and found that, the inclusion of nanoparticles into the base fluid is capable of varying the flow pattern. Turkyilmazoglu [32] reported the exact solution for heat and mass transfer of magnetohydrodynamic flow of nanofluid. Further, Turkyilmazoglu and Pop [33] have examined the heat and mass transfer of unsteady natural convection flow of nanofluid past a vertical infinite plate with thermal radiation. Das [34] discussed the problem of free convection flow of nanofluid bounded by moving vertical plate with constant heat source and convective boundary condition in a rotating frame of reference. He found that, the skin friction coefficient increases with an increase in the nanoparticle volume fraction. Recently, Sheikholeslami and Ganji [35] have presented the heat and mass transfer behavior of unsteady flow of nanofluid between parallel plates in the presence of thermal radiation. They conclude that, the solutal boundary layer thickness increases with increase in radiation parameter. Freidoonimehr et al. [36] presented the analytical solution for three-dimensional squeezing nanofluid flow in a rotating channel using Tiwari and Das model. With the aid of same model Gireesha et al. [37] have studied the effect of nanoparticles on flow and heat transfer of dusty fluid. Das et al. [38] have found that the volume fraction parameter decreases the rate of heat transfer in a fully developed mixed convection flow through a vertical channel filled with water based nanofluid with the uniform transverse magnetic field. Das and Jana [39] studied the MHD flow past a moving vertical plate in the presence of thermal radiation using Laplace transform method for closed form expressions of flow fields. Also, they found that, the shear stress at the plate for Cu–water nanofluid is found to be lower. Heat transfer in flow of nanofluid with heat source/sink and an induced magnetic field is addressed by Gireesha et al. [40].

An Extension to this topic, Sheikholeslami et al. [41–44] added a new dimension to the study of nanofluid flow in channel/different geometry under diverse physical aspects by using single/two-phase model. Motivated by aforementioned studies, we intend to investigate combined effects of heat and mass transfer on natural convection flow of water based nanofluid over a stationary/moving vertical plate. The effects of heat source/sink, chemical reaction and thermal radiation are also considered. To the best of our knowledge, this study has not been considered by any authors. Hence, the novelty of this study is to obtain the closed form solution for the present problem by employing Laplace transform technique. The basic nonlinear partial differential equations are derived by using Boussinesq approximation and then are transformed to dimensionless equations using suitable non-dimensional variables. The resultant equations have been solved analytically.

2. Mathematical formulation and solution

Consider an unsteady, laminar flow of nanofluid over an infinite stationary/moving vertical flat plate. The plate is at rest initially with constant ambient temperature and concentration. The plate starts to move vertically with the velocity λu_0 for $t > 0$. The temperature and concentration are raised or lowered to T_w and C_w correspondingly. The magnetic Reynolds number is assumed to be so small, so that the induced magnetic field and Hall current are negligible. The governing equations of conservation of mass, momentum, energy and concentration of nanofluid are given by the following:

$$\nabla \cdot \boldsymbol{U} = 0, \tag{2.1}$$

$$\rho_{nf}\frac{\partial \boldsymbol{U}}{\partial t} = -\nabla p + \mu_{nf}\nabla^2 \boldsymbol{U} + \boldsymbol{J} \times \boldsymbol{B} + gb, \tag{2.2}$$

Table 1 Thermo-physical properties of water and copper nanoparticles [39].

Physical properties	Water/base fluid	Cu (copper)
ρ (kg/m^3)	997.1	8933
c_p (J/kg K)	4179	385
k (W/m K)	0.613	401
$\beta_t \times 10^5$ (K^{-1})	21	1.67
$\beta_c \times 10^6$ (m^2/h)	298.2	3.05
σ (s/m)	5.5×10^{-6}	59.6×10^6

$$\left(\rho c_p\right)_{nf}\frac{\partial T}{\partial t} = -\nabla \cdot q, \tag{2.3}$$

$$\frac{\partial C}{\partial t} = -\nabla \cdot j, \tag{2.4}$$

where $\boldsymbol{U} = (u, v, w)$ is the velocity vector, ρ_{nf} the effective density of nanofluid, μ_{nf} the effective dynamic viscosity of nanofluid, ∇p the pressure gradient, $\boldsymbol{B}$ the magnetic field, g the acceleration due to gravity, b the body forces, T the temperature, $\left(c_p\right)_{nf}$ the effective specific heat, $q = -k_{nf}\nabla T$ the heat flux, C the concentration, $j = -D\nabla C$ the mass flux, k_{nf} the effective thermal conductivity, D the diffusion co-efficient, t the time and $\boldsymbol{J} = \sigma_{nf}(\boldsymbol{E} + \boldsymbol{U} \times \boldsymbol{B})$ the current density.

The x-axis is taken along the plate in the vertically upward direction and y-axis is normal to it. In the plane $y = 0$ the plate coincides and the flow being confined to $y > 0$ as shown in Fig. 1. A uniform transverse magnetic field of strength B_0 and radiative heat flux q_r are applied normal to the flow direction and it is assumed that there is no applied or polarization voltage exists. It is assumed that the pressure gradient is neglected and the fluid is electrically conducting, water based nanofluid embedded with copper nanoparticles. Further, it is considered as, the base fluid and suspended nanoparticles are in thermal equilibrium. In Table 1, the thermo-physical properties of nanofluid are presented. The 1st order chemical reaction between the nanofluid and the species concentration is taken into the account. The reaction is assumed to take place entirely in the stream.

Under aforementioned assumptions and usual Boussinesq's approximation, the governing equations in its component form readily read as [39];

$$\rho_{nf}\frac{\partial u}{\partial t} = \mu_{nf}\frac{\partial^2 u}{\partial y^2} - \sigma_{nf}B_0^2 u + g(\rho\beta_T)_{nf}(T - T_\infty) + g(\rho\beta_C)_{nf}(C - C_\infty), \tag{2.5}$$

$$\left(\rho c_p\right)_{nf}\frac{\partial T}{\partial t} = k_{nf}\frac{\partial^2 T}{\partial y^2} - \frac{\partial q_r}{\partial y} + Q_0(T - T_\infty), \tag{2.6}$$

$$\frac{\partial C}{\partial t} = D\frac{\partial^2 C}{\partial y^2} - k_1(C - C_\infty), \tag{2.7}$$

where σ_{nf} is the effective electrical conductivity, $\beta_{T_{nf}}$ the effective thermal volumetric coefficient of expansion, $\beta_{C_{nf}}$ the effective solutal volumetric coefficient of expansion, k_1 the chemical reaction coefficient and Q_0 the uniform volumetric heat source/sink. The effective properties of nanofluid are given by following co-relations (see Das and Jana [39]);

$$\begin{aligned}
&\mu_{nf} = \frac{\mu_f}{(1-\phi)^{2.5}}, \quad \rho_{nf} = (1-\phi)\rho_f + \phi\rho_s, \\
&\left(\rho c_p\right)_{nf} = (1-\phi)\left(\rho c_p\right)_f + \phi\left(\rho c_p\right)_s, \\
&(\rho\beta_T)_{nf} = (1-\phi)(\rho\beta_T)_f + \phi(\rho\beta_T)_s, \\
&(\rho\beta_C)_{nf} = (1-\phi)(\rho\beta_C)_f + \phi(\rho\beta_C)_s, \\
&\sigma_{nf} = \sigma_f\left[1 + \frac{3(\sigma-1)\phi}{\sigma+2-(\sigma-1)\phi}\right], \\
&\sigma = \frac{\sigma_s}{\sigma_f}, \quad \frac{k_{nf}}{k_f} = \frac{k_s + 2k_f - 2\phi\left(k_f - k_s\right)}{k_s + 2k_f + \phi\left(k_f - k_s\right)},
\end{aligned} \tag{2.8}$$

where ϕ-the volume fraction of nanoparticles, ρ_f and ρ_s are density of base fluid and nanoparticles respectively, c_{p_f} and c_{p_s}-specific heat of the base fluid and nanoparticles respectively, σ_f and σ_s are the electrical conductivity of base fluid and nanoparticles correspondingly, β_{T_f} and β_{T_s} are thermal volumetric coefficient of the base fluid and nanoparticles correspondingly, β_{C_f} and β_{C_s} are solutal volumetric coefficient of the base fluid and nanoparticles correspondingly, and k_f and k_s are thermal conductivity of base fluid and nanoparticles respectively.

The appropriate initial and boundary conditions of the present problem are

$$\begin{aligned}
&t = 0: u = 0, \quad T = T_\infty, \quad C = C_\infty \quad \text{for all} \quad y \geqslant 0, \\
&t > 0: u = \lambda u_0, \quad T = T_w, \quad C = C_w \quad \text{at} \quad y = 0, \\
&t > 0: u \to 0, \quad T \to T_\infty, \quad C \to C_\infty \quad \text{as} \quad y \to \infty,
\end{aligned} \tag{2.9}$$

where λ is the direction of plate movement. It is worth to mention that, $\lambda = 0$ corresponds to stationary plate and $\lambda \neq 0$ corresponds to moving plate. Now by using Rosseland approximation, the radiative heat flux q_r can be expressed as (see Sheikholeslami and Ganji [24]);

$$q_r = -\frac{4\sigma^*}{3k^*}\frac{\partial T^4}{\partial y}, \tag{2.10}$$

where σ^* is the Stefan Boltzmann constant and k^* is the Rosseland mean absorption co-efficient. Now by assuming small temperature difference with the flow, the temperature can be expressed as a linear function of temperature, and this is by employing Taylor series to expand the T^4 about T_∞ as follows:

$$T^4 = T_\infty^4 + 3T_\infty^3(T - T_\infty) + 6T_\infty^2(T - T_\infty)^2 + \cdots \tag{2.11}$$

Beyond the first order, neglecting the higher order terms in the above equation, one can get;

$$T^4 \approx 4T_\infty^3 T - 3T_\infty^4. \tag{2.12}$$

In the view of Eqs. (2.10) and (2.12), the Eq. (2.6) will take the following form;

$$\left(\rho c_p\right)_{nf}\frac{\partial T}{\partial t} = k_{nf}\frac{\partial^2 T}{\partial y^2} + \frac{16\sigma^* T_\infty^3}{3k^*}\frac{\partial^2 T}{\partial y^2} + Q_0(T - T_\infty). \tag{2.13}$$

It is opportune to non-dimensionalize the equations by employing following variables;

$$\eta=\frac{u_0 y}{\nu_f},\quad \tau=\frac{u_0^2 t}{\nu_f},\quad f=\frac{u}{u_0},\quad \theta=\frac{T-T_\infty}{T_w-T_\infty},\quad \varphi=\frac{C-C_\infty}{C_w-C_\infty},$$
$$M^2=\frac{\sigma_f B_0^2 \nu_f}{u_0\rho_f},\quad Grt=\frac{g\beta_{Tf}(T_w-T_\infty)\nu_f}{u_0^3},\quad Grc=\frac{g\beta_{Cf}(C_w-C_\infty)\nu_f}{u_0^3},$$
$$Pr=\frac{(\mu c_p)_f}{k_f},\quad R=\frac{4\sigma^* T_\infty^3}{k^* k_f},\quad Q=\frac{Q_0\nu_f}{u_0^2(\rho c_p)_f},\quad Sc=\frac{D}{\nu_f},\quad K=\frac{k_1\nu_f}{u_0^2}. \tag{2.14}$$

On substituting these dimensionless variables into the governing equations and boundary conditions, one can get;

$$\frac{\partial f}{\partial\tau}=a_1\frac{\partial^2 f}{\partial\eta^2}+Grta_2\theta+Grca_3\varphi-M^2 a_4 f, \tag{2.15}$$

$$\frac{\partial\theta}{\partial\tau}=a_5\frac{\partial^2\theta}{\partial\eta^2}+a_6\theta, \tag{2.16}$$

$$\frac{\partial\varphi}{\partial\tau}=\frac{1}{Sc}\frac{\partial^2\varphi}{\partial\eta^2}-K\varphi, \tag{2.17}$$

with

$$\begin{aligned}&\tau=0: f=0,\quad \theta=0,\quad \varphi=0\quad \forall\eta\geqslant 0,\\ &\tau>0: f=\lambda,\quad \theta=1,\quad \varphi=1\quad \text{at}\quad \eta=0,\\ &\tau>0: f\to 0,\quad \theta\to 0,\quad \varphi\to 0\quad \text{as}\quad \eta\to\infty.\end{aligned} \tag{2.18}$$

By applying Laplace transform on both sides of Eqs. (2.15)–(2.18), we have;

$$a_1\frac{\partial^2\bar f}{\partial\eta^2}+Grta_2\bar\theta+Grca_3\bar\varphi-(M^2 a_4+s)\bar f=0, \tag{2.19}$$

$$a_5\frac{\partial^2\bar\theta}{\partial\eta^2}+(a_6-s)\bar\theta=0, \tag{2.20}$$

$$\frac{1}{Sc}\frac{\partial^2\bar\varphi}{\partial\eta^2}-(K+s)\bar\varphi=0, \tag{2.21}$$

With corresponding initial and boundary conditions are

$$\begin{aligned}&\bar f=0,\quad \bar\theta=0,\quad \bar\varphi=0\quad \forall\eta\geqslant 0\\ &\bar f=\frac{\lambda}{s},\quad \bar\theta=\frac{1}{s},\quad \bar\varphi=\frac{1}{s}\quad \text{at}\quad \eta=0\\ &\bar f\to 0,\quad \bar\theta\to 0,\quad \bar\varphi\to 0\quad \text{as}\quad \eta\to\infty\end{aligned} \tag{2.22}$$

where $\bar f=\int_0^\infty f(\tau,\eta)e^{-s\tau}d\tau$, $\bar\theta=\int_0^\infty \theta(\tau,\eta)e^{-s\tau}d\tau$, $\bar\varphi=\int_0^\infty \varphi(\tau,\eta)e^{-s\tau}d\tau$ and $s>0$. Now by solving above system, one can have;

$$\bar\varphi(\eta,s)=\frac{1}{s}e^{-\sqrt{Sc(s+K)}\eta}, \tag{2.23}$$

$$\bar\theta(\eta,s)=\frac{1}{s}e-\sqrt{\frac{s-a_6}{a_5}}\eta, \tag{2.24}$$

$$\begin{aligned}\bar f(\eta,s)=&\frac{\lambda}{s}e^{-\sqrt{\frac{s+a_9}{a_1}}\eta}\\ &+\frac{Grta_7}{b1}\left\{\frac{1}{s-b_1}-\frac{1}{s}\right\}\left(e^{-\sqrt{\frac{s+a_9}{a_1}}\eta}-e^{-\sqrt{\frac{s-a_6}{a_5}}\eta}\right)\\ &+\frac{Grca_8}{b2}\left\{\frac{1}{s-b_2}-\frac{1}{s}\right\}\left(e^{-\sqrt{\frac{s+a_9}{a_1}}\eta}-e^{-\sqrt{Sc(s+K)}\eta}\right).\end{aligned} \tag{2.25}$$

Table 2 The numerical values of skin friction co-efficient for various values of M^2, ϕ, Grt, Grc and τ when $R=2,\ Q=-1,\ Pr=6.2,\ Sc=0.6$ and $K=5$.

M^2	ϕ	Grt	Grc	τ	$C_f\ \lambda=0$	$C_f\ \lambda\neq 0$
0	0.2	10	10	0.5	−7.69E + 03	−7.70E + 03
1					26.7770	25.4943
1.5					4.4823	3.0559
2					3.2406	1.6775
2.5					3.2703	1.5767
1	0				4.9185	3.7519
	0.05				6.1722	4.9443
	0.1				7.4002	6.1350
	0.15				10.0833	8.8008
	0.2				26.7770	25.4943
		−4			20.3474	1.91E + 01
		−2			21.2659	19.9832
		0			22.1844	20.9017
		2			23.1029	21.8203
		4			24.0214	22.7388
			−4		−4.2812	−5.5639
			−2		0.1557	−1.1270
			0		4.5926	3.3099
			2		9.0295	7.7468
			4		13.4663	12.1837
				0.1	6.4963	4.1781
				0.2	10.2000	8.4604
				0.3	14.3132	12.8126
				0.4	19.5713	18.2037
				0.5	26.7770	25.4943

In order to determine, the flow fields in the time domain, by applying inverse Laplace transform on both sides of (2.23)–(2.25), we get;

$$\begin{aligned}f(\eta,\tau)=&\lambda f_1(\eta,\tau,a_1,a_9)+\frac{Grta_7}{b1}\{f_2(\eta,\tau,a_1,a_9,b_1)\\ &-f_3(\eta,\tau,a_5,a_6,b_1)-f_1(\eta,\tau,a_1,a_9)+f_4(\eta,\tau,a_5,a_6)\},\\ &+\frac{Grca_8}{b2}\{f_5(\eta,\tau,a_1,a_9,b_2)-f_6(\eta,\tau,Sc,K,b_2)\\ &-f_1(\eta,\tau,a_1,a_9)+f_7(\eta,\tau,Sc,K)\}\end{aligned} \tag{2.26}$$

$$\theta(\eta,\tau)=f_4(\eta,\tau,a_5,a_6), \tag{2.27}$$

$$\varphi(\eta,\tau)=f_7(\eta,\tau,Sc,K), \tag{2.28}$$

where

$$x_1=(1-\phi)+\phi\frac{\rho_s}{\rho_f},\quad x_2=(1-\phi)+\phi\frac{(\rho\beta_T)_s}{(\rho\beta_T)_f},$$

$$x_3=(1-\phi)+\phi\frac{(\rho\beta_c)_s}{(\rho\beta_c)_f},\quad x_4=\left[1+\frac{3(\sigma-1)\phi}{\sigma+2-(\sigma-1)\phi}\right],\quad \sigma=\frac{\sigma_s}{\sigma f},$$

$$x_5=(1-\phi)+\phi\frac{(\rho c_p)_s}{(\rho c_p)_f},$$

$$x_6=\frac{k_{nf}}{k_f}=\left[\frac{k_s+2k_f-2\phi(k_f-k_s)}{k_s+2k_f+\phi(k_f-k_s)}\right],$$

Table 3 The numerical values of Nusselt number and skin friction co-efficient for various values of Pr when $R = 2,\ Q = -1,\ M^2 = 1,\ Grt = Grc = 4,\ \tau = 0.5,\ Sc = 0.6$ and $K = 5$.

Pr	Ordinary fluid ($\phi = 0$)		Nanofluid ($\phi \neq 0$)	
	Nu	C_f	Nu	C_f
6.2	1.6771	3.7519	1.4901	25.4943
10	2.1300	3.3672	1.8924	4.0267
20	3.0122	2.8571	2.6762	2.6724
50	4.7628	2.2944	4.2315	1.8037
100	6.7355	1.9591	5.9842	1.3685
200	9.5255	1.6961	8.4630	1.0469
1000	21.2997	1.3057	18.9238	0.5884

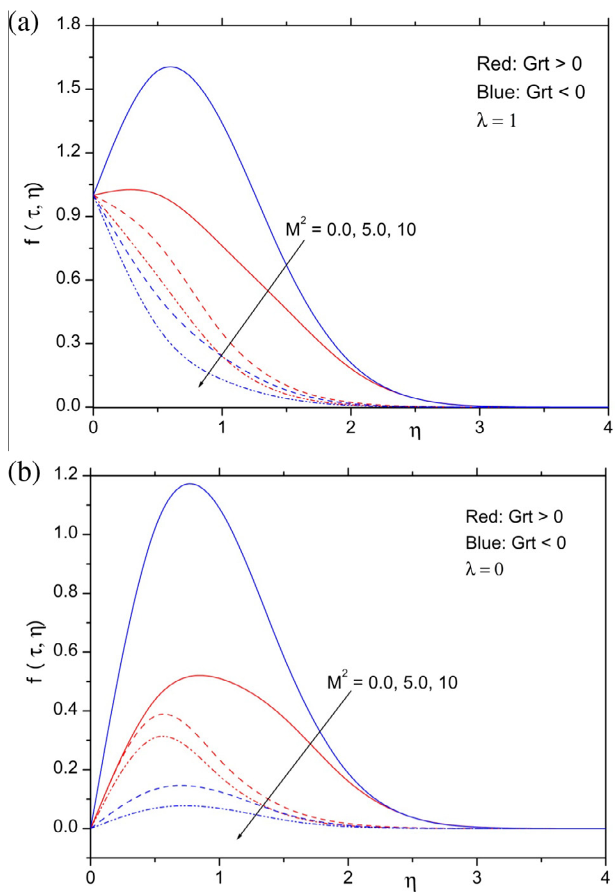

Fig. 2 The effect of magnetic parameter on velocity profiles for (a) moving plate and (b) stationary plate in both $Grt > 0$ and $Grt < 0$ cases.

$$a_1 = \frac{1}{(1-\phi)^{2.5}x_1},\quad a_2 = \frac{x_2}{x_1},\quad a_3 = \frac{x_3}{x_1},\quad a_4 = \frac{x_4}{x_1},$$

$$a_5 = \frac{1}{x_5 Pr}\left\{x_6 + \frac{3}{4}R\right\},\quad a_6 = \frac{Q}{x_5},\quad a_7 = \frac{a_2 a_5}{a_1 - a_5},\quad a_8 = \frac{a_3}{a_1 - Sc},$$

$$a_9 = M^2 a_4,\quad b_1 = \frac{a_1 a_6 + M^2 a_4 a_5}{a_1 - a_5},\quad b_2 = \frac{M^2 a_4 Sc - a_1 K}{a_1 - Sc},$$

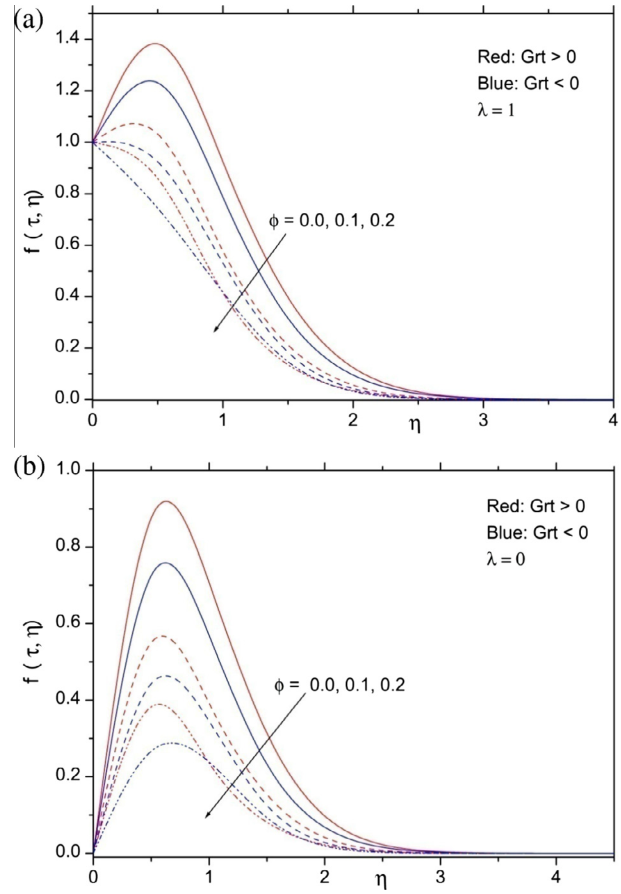

Fig. 3 The effect of nanoparticle volume fraction parameter on velocity profiles for (a) moving plate and (b) stationary plate in both $Grt > 0$ and $Grt < 0$ cases.

$$f_1(\eta,\tau,a_1,a_9) = \frac{1}{2}\left\{e^{\sqrt{\frac{a_9}{a_1}}\eta} erfc\left(\frac{\eta}{2\sqrt{\tau a_1}} + \sqrt{a_9\tau}\right) + e^{-\sqrt{\frac{a_9}{a_1}}\eta} erfc\left(\frac{\eta}{2\sqrt{\tau a_1}} - \sqrt{a_9\tau}\right)\right\},$$

$$f_2(\eta,\tau,a_1,a_9,b_1) = \frac{e^{b_1\tau}}{2}\left\{e^{\sqrt{\frac{a_9+b_1}{a_1}}\eta} erfc\left(\frac{\eta}{2\sqrt{\tau a_1}} + \sqrt{(a_9+b_1)\tau}\right) + e^{-\sqrt{\frac{a_9+b_1}{a_1}}\eta} erfc\left(\frac{\eta}{2\sqrt{a_1\tau}} - \sqrt{(a_9+b_1)\tau}\right)\right\},$$

$$f_3(\eta,\tau,a_5,a_6,b_1) = \frac{e^{b_1\tau}}{2}\left\{e^{\sqrt{\frac{b_1-a_6}{a_5}}\eta} erfc\left(\frac{\eta}{2\sqrt{\tau a_5}} + \sqrt{(b_1-a_6)\tau}\right) + e^{-\sqrt{\frac{b_1-a_6}{a_5}}\eta} erfc\left(\frac{\eta}{2\sqrt{a_5\tau}} - \sqrt{(b_1-a_6)\tau}\right)\right\},$$

$$f_4(\eta,\tau,a_5,a_6) = \frac{1}{2}\left\{e^{\sqrt{-\frac{a_6}{a_5}}\eta} erfc\left(\frac{\eta}{2\sqrt{\tau a_5}} + \sqrt{-a_6\tau}\right) + e^{-\sqrt{-\frac{a_6}{a_5}}\eta} erfc\left(\frac{\eta}{2\sqrt{\tau a_5}} - \sqrt{-a_6\tau}\right)\right\},$$

$$f_5(\eta,\tau,a_1,a_9,b_2) = \frac{e^{b_2\tau}}{2}\left\{e^{\sqrt{\frac{a_9+b_2}{a_1}}\eta} erfc\left(\frac{\eta}{2\sqrt{\tau a_1}} + \sqrt{(a_9+b_2)\tau}\right) + e^{-\sqrt{\frac{a_9+b_2}{a_1}}\eta} erfc\left(\frac{\eta}{2\sqrt{a_1\tau}} - \sqrt{(a_9+b_2)\tau}\right)\right\},$$

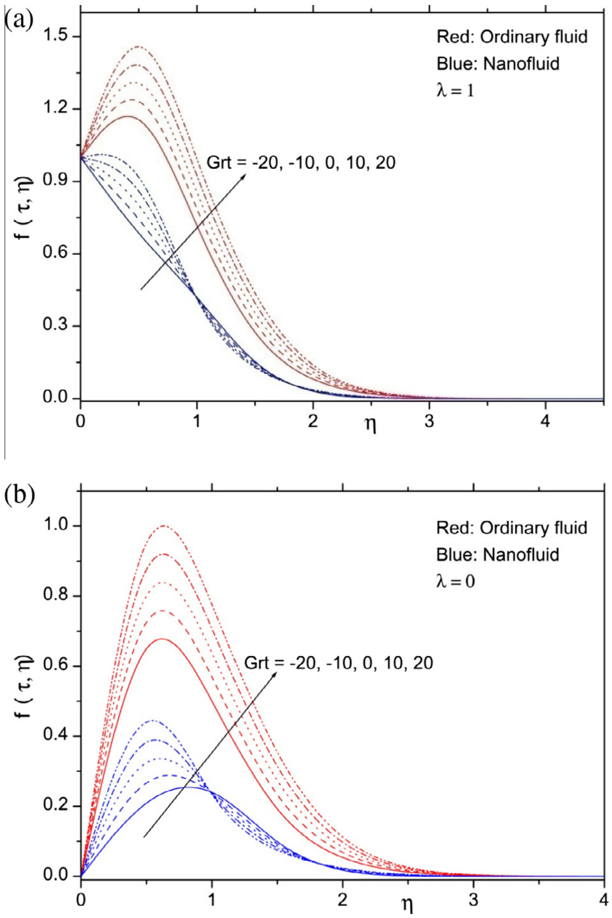

Fig. 4 The effect of thermal Grashof number on velocity profiles for (a) moving plate and (b) stationary plate in both $\phi = 0$ and $\phi \neq 0$ cases.

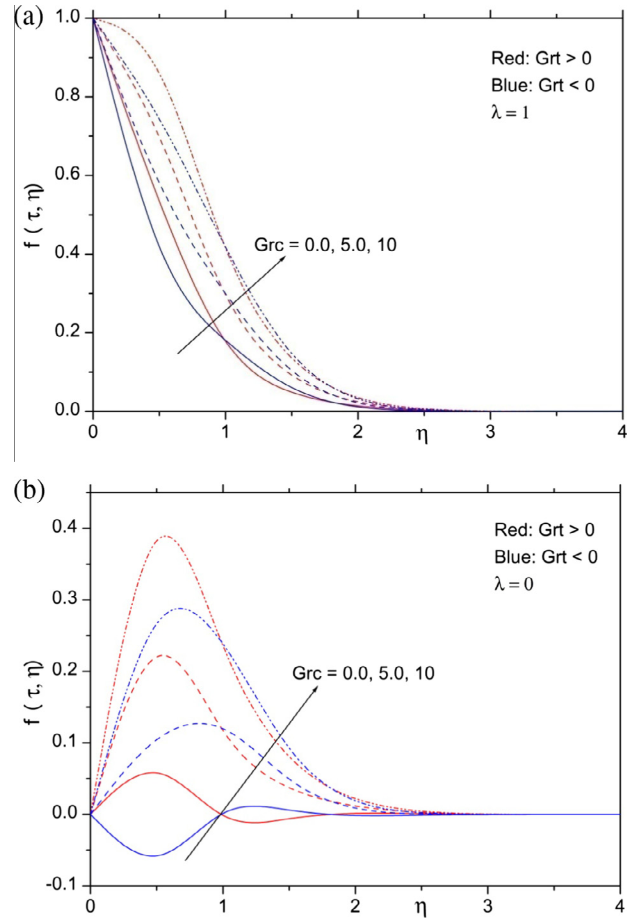

Fig. 5 The effect of solute Grashof number on velocity profiles for (a) moving plate and (b) stationary plate in both $Grt > 0$ and $Grt < 0$ cases.

$$f_6(\eta,\tau,Sc,K,b_2)=\frac{e^{b_2\tau}}{2}\left\{\begin{array}{l} e^{\sqrt{\frac{K+b_2}{Sc}}\eta} erfc\left(\frac{\eta}{2\sqrt{\tau sc}}+\sqrt{(K+b_2)\tau}\right)+e^{-\sqrt{\frac{K+b_2}{Sc}}\eta} \\ erfc\left(\frac{\eta}{2\sqrt{Sc\tau}}-\sqrt{(K+b_2)\tau}\right)\end{array}\right\},$$

$$f_7(\eta,\tau,Sc,K)=\frac{1}{2}\left\{e^{\sqrt{\frac{K}{Sc}}\eta} erfc\left(\frac{\eta}{2\sqrt{\tau Sc}}+\sqrt{K\tau}\right)+e^{-\sqrt{\frac{K}{Sc}}\eta} erfc\left(\frac{\eta}{2\sqrt{Sc\tau}}-\sqrt{K\tau}\right)\right\},$$

Here $erfc(\cdot)$ is complementary error function and is defined as $erfc(x)=\frac{2}{\sqrt{\pi}}\int_x^\infty e^{-t^2}dt$. The skin friction coefficient, Nusselt number and Sherwood number are most important physical quantities in the point of engineering interest. The skin friction coefficient at the plate $\eta = 0$ is given by;

$$C_f = \left.\frac{\partial f(\eta,\tau)}{\partial \eta}\right|_{\eta=0},$$

$$C_f = \lambda g_1 + \frac{Grta_7}{b1}\{g_2 - g_3 - g_1 + g_4\} + \frac{Grca_8}{b2}\{g_5 - g_6 - g_1 + g_7\}, \quad (2.29)$$

here $g_1 = \left(-\sqrt{\frac{a_9}{a_1}} erf\sqrt{a_9\tau} - \frac{1}{\sqrt{\tau a_1 \pi}} e^{-a_9\tau}\right),$

$$g_2 = -e^{b_1\tau}\left(\sqrt{\frac{a_9+b_1}{a_1}} erf\sqrt{(a_9+b_1)\tau} + \frac{1}{\sqrt{\tau a_1\pi}} e^{-(a_9+b_1)\tau}\right),$$

$$g_3 = -e^{b_1\tau}\left(\sqrt{\frac{b_1-a_6}{a_5}} erf\sqrt{(b_1-a_6)\tau} + \frac{1}{\sqrt{\tau a_5\pi}} e^{-(b_1-a_6)\tau}\right),$$

$$g_4 = -\left(\sqrt{\frac{-a_6}{a_5}} erf\sqrt{-a_6\tau} + \frac{1}{\sqrt{\tau a_5\pi}} e^{a_6\tau}\right),$$

$$g_5 = -e^{b_2\tau}\left(\sqrt{\frac{a_9+b_2}{a_1}} erf\sqrt{(a_9+b_2)\tau} + \frac{1}{\sqrt{\tau a_1\pi}} e^{-(a_9+b_2)\tau}\right),$$

$$g_6 = -e^{b_2\tau}\left(\sqrt{\frac{K+b_2}{Sc}} erf\sqrt{(K+b_2)\tau} + \frac{1}{\sqrt{\tau\pi Sc}} e^{-(K+b_2)\tau}\right),$$

$$g_7 = -\left(\sqrt{\frac{K}{Sc}} erf\sqrt{K\tau} + \frac{1}{\sqrt{\tau\pi Sc}} e^{-K\tau}\right).$$

where $erf(\cdot)$ is the error function and is defined as $erf(x)=\frac{2}{\sqrt{\pi}}\int_0^x e^{-t^2}dt$. The Nusselt number is given by;

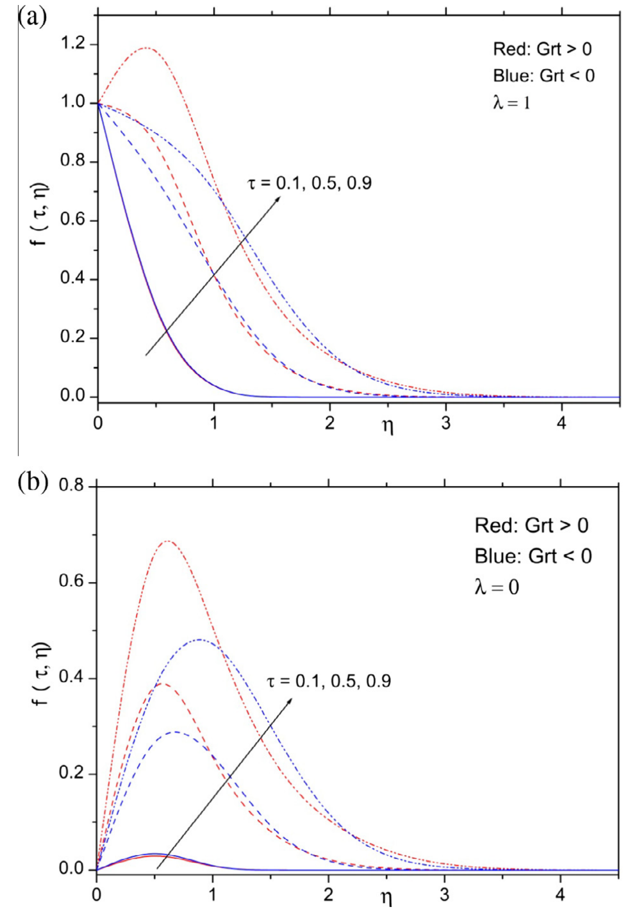

Fig. 6 The effect of time parameter on velocity profiles for (a) moving plate and (b) stationary plate in both $Grt > 0$ and $Grt < 0$ cases.

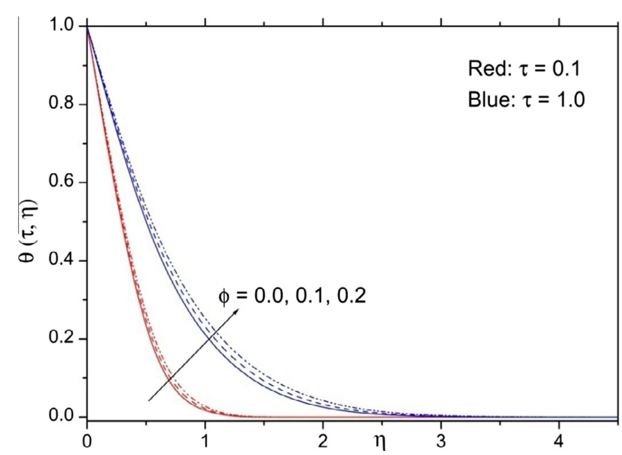

Fig. 7 The effect of nanoparticle volume fraction parameter on temperature profile.

$$Nu = -\frac{\partial\theta(\eta,\tau)}{\partial\eta}\bigg|_{\eta=0},$$

$$Nu = \sqrt{\frac{-a_6}{a_5}}erf\sqrt{-a_6\tau} + \frac{1}{\sqrt{\tau a_5\pi}}e^{a_6\tau}, \tag{2.30}$$

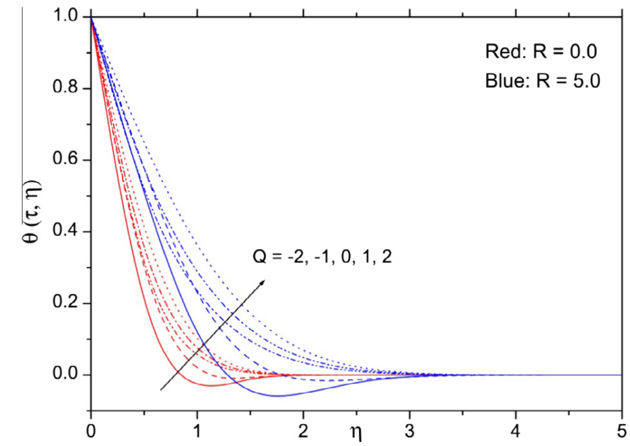

Fig. 8 The effect of heat source/sink parameter on temperature profile.

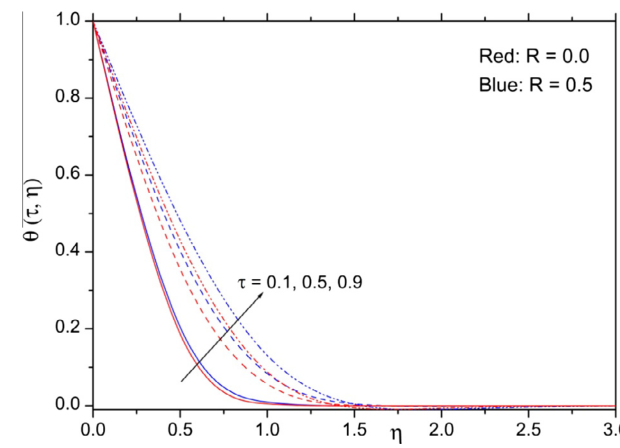

Fig. 9 The effect of time parameter on temperature profile.

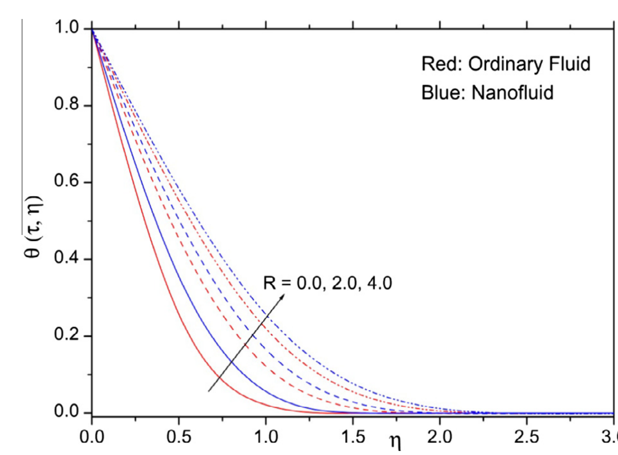

Fig. 10 The effect of radiation parameter on temperature profile.

The Sherwood number is defined as

$$Sh = -\frac{\partial\varphi(\eta,\tau)}{\partial\eta}\bigg|_{\eta=0},$$

$$Sh = \sqrt{\frac{K}{Sc}}\,erf\sqrt{K\tau} + \frac{1}{\sqrt{\tau\pi Sc}}e^{-K\tau}. \tag{2.31}$$

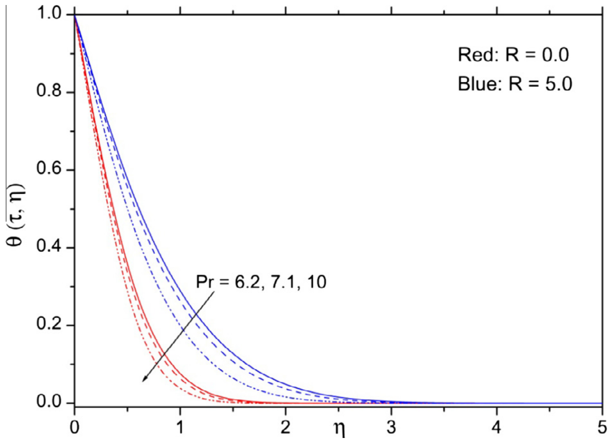

Fig. 11 The effect of Prandtl number on temperature profile.

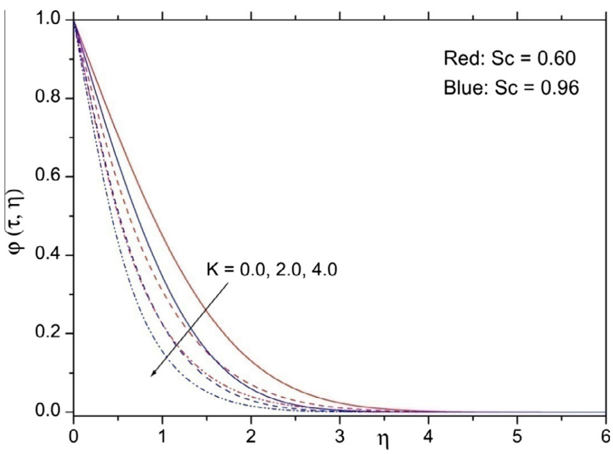

Fig. 12 The effect of chemical reaction parameter on concentration profile.

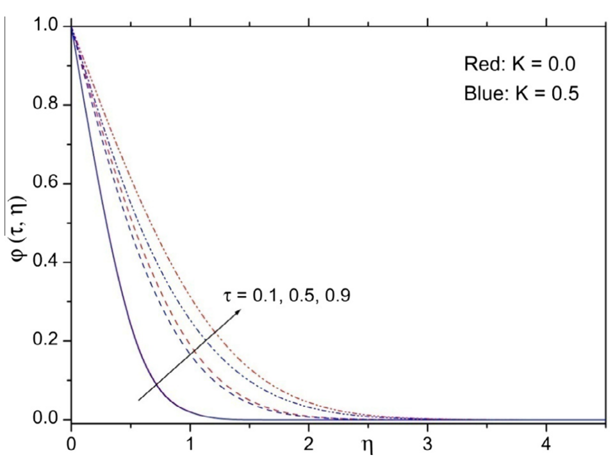

Fig. 13 The effect of time parameter on concentration profile.

It is worth to mention that, by neglecting heat source/sink, chemical reaction and mass transfer effects, the solutions of the present study are identical to Das and Jana [39].

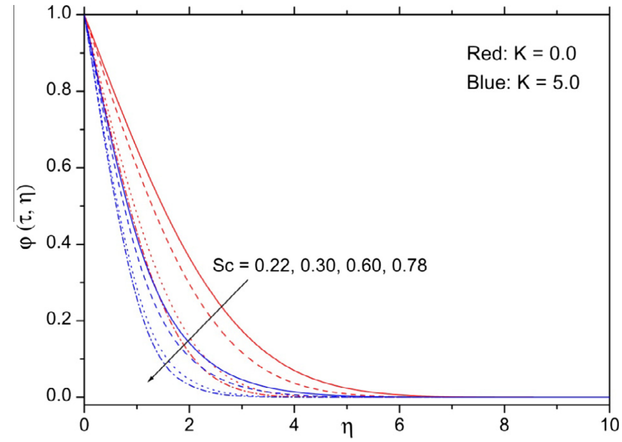

Fig. 14 The effect of Schmidt number on concentration profile.

3. Result and discussion

In the present study, the Laplace transform scheme has been employed to obtain the analytical expressions for velocity, temperature and concentration profiles as well as the skin friction coefficient, Nusselt number and Sherwood number. In order to analyze the salient features of different flow fields, a numerical computation is carried out for different values of pertinent parameter. The results of numerical computation are presented through graphs 2–18 and in Tables 2 and 3. The values of thermo-physical properties of base fluid (water) and nanoparticle (copper) are taken from the data presented in Table 1. The range of nanoparticle volume fraction is chosen as $0 \leqslant \phi \leqslant 0.2$. The value of Prandtl number is taken as 6.2, which physically corresponds to base fluid (water). It is worth to mention that, $Gr > 0$ and $Gr < 0$ means that the cooling and heating of the plate by free convection current correspondingly and $Gr = 0$ correspond to the absence of free convection current. Throughout our numerical computation, we have chosen other parameters as $\tau = M^2 = 0.5$, $R = 2$, $Q = 1$, $Sc = 0.6$, $Grt = Grc = 10$ and $K = 0.5$ unless otherwise stated.

The impact of magnetic field on the dimensionless velocity profile is depicted in Fig. 2 for both stationary and moving plate case. From Fig. 2, it is observed that, an increase in magnetic parameter leads to decrease in the velocity profile in both $Gr > 0$ and $Gr < 0$ cases. This is due to the fact that, the application of transverse magnetic field to an electrically conducting fluid gives rise to a resistive type of force called the Lorentz force. This force has the tendency to slow down the motion of the fluid; consequently, the fluid velocity decreases significantly. This outcome is consistently agreed with that of Sheikholeslami and Ganji [44]. Fig. 3 depicts the variation of dimensionless velocity profiles f versus η for different values of the nanoparticle volume fraction parameter in both $Gr > 0$ and $Gr < 0$ cases. By increasing nanoparticle volume fraction parameter results in an increase in the friction force within the fluid. As a consequence the velocity field decreases in both moving and stationary plates. It is also observed that, the momentum of the fluid is lower in the case of $Gr > 0$ than that of $Gr < 0$.

The inclusion of buoyancy effects is illustrated in Figs. 4 and 5. The occurrence of buoyancy influences complicates

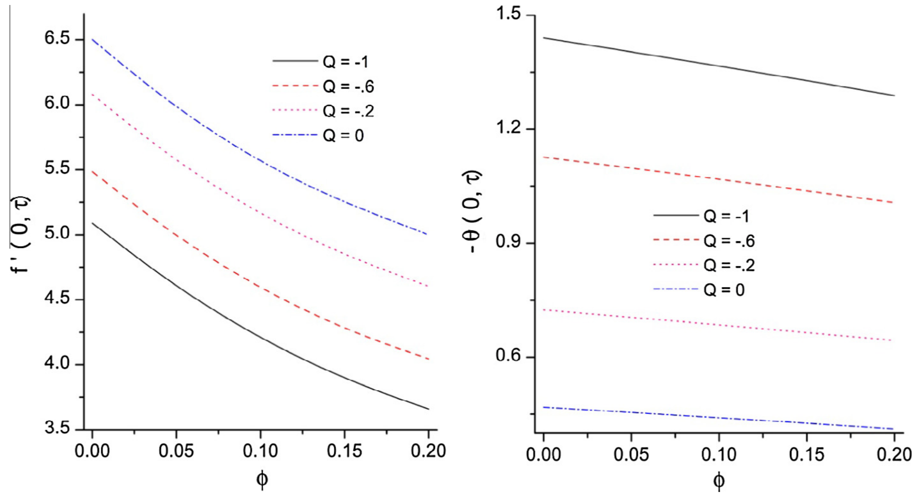

Fig. 15 The effect of heat source/sink parameter on skin friction and Nusselt number profiles.

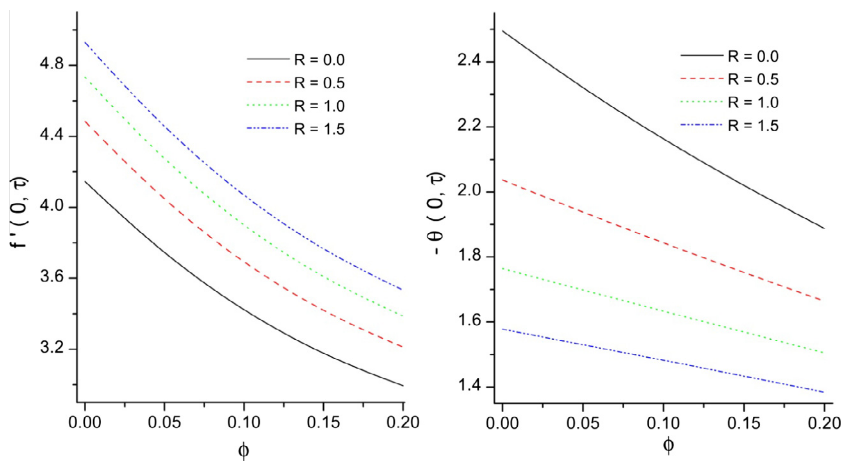

Fig. 16 The effect of radiation parameter on skin friction and Nusselt number profiles.

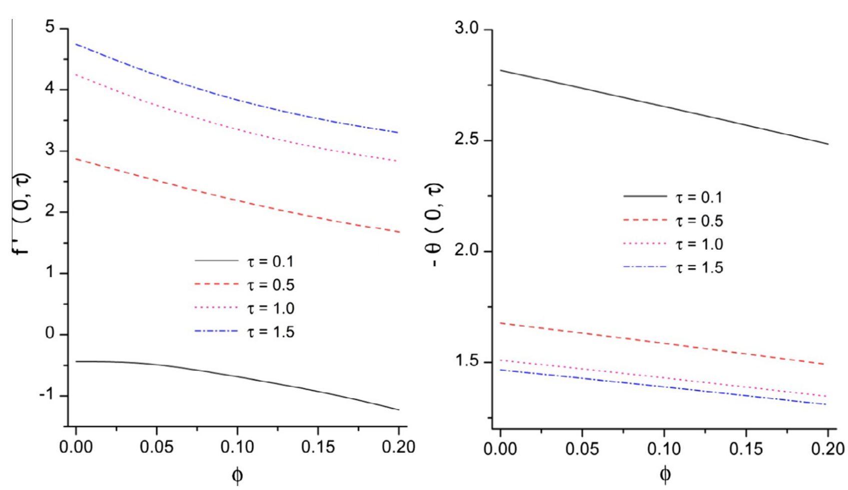

Fig. 17 The effect of time parameter on skin friction and Nusselt number profiles.

the flow analysis with thermal and solutal analysis. From Fig. 4 it is noticed that, the velocity increases in the neighborhood of the plate by increasing the thermal Grashof number. But this trend is qualitatively opposite at the long distance from the plate. Physically speaking, the thermal Grashof number signifies the relative importance of buoyancy force to the viscous hydrodynamic force. The larger Grashof number indicates lower viscous effects in momentum equation.

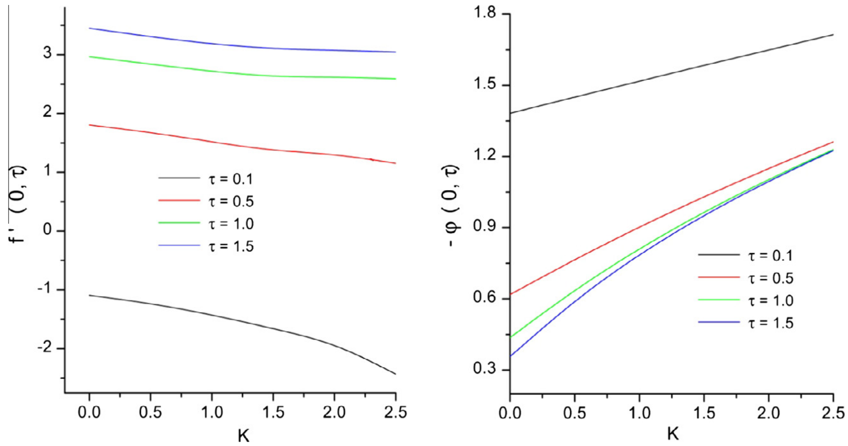

Fig. 18 The effect of time parameter on skin friction and Sherwood number profiles.

Accordingly, the momentum of the fluid is higher. It is also observed that, the velocity of ordinary fluid is large when compared to the nanofluid velocity. On the other hand, an expected outcome was obtained for the influence of solutal Grashof number in both cases. That is, the fluid velocity gets enhanced due to increase in the species buoyancy force, which is as shown in Fig. 5. The solutal Grashof number is described as the ratio of the species buoyancy force to the viscous hydrodynamic force. As solutal Grashof number increases, the viscous hydrodynamic force decreases. As a result, the momentum boundary layer thickens. In Fig. 6, we can observe that an increase in time leads to an increase in the velocity profile in both the cases. Importantly, the behavior of velocity profile noticed in Figs. 2–6 is qualitatively same in both moving and stationary plates.

The effect of nanoparticle volume fraction, heat source/sink, time parameter, thermal radiation and Prandtl number on the dimensionless temperature profile versus η has been plotted in Figs. 7–11 correspondingly. It is observed in Fig. 7 that, an increase in the volume fraction parameter leads to an intensification of the temperature profile. Strengthening of volume fraction of nanoparticles enhances the thermal conductivity of the nanofluid and as a result the thermal boundary layer thickens. The volume fraction parameter is a key parameter and it has a significant role in the improvement of heat characteristics of the fluids. Thus we can conclude that, the temperature can be controlled by varying the nanoparticle volume fraction in many industrial processes. It is also observed that, the temperature profile is higher for larger time ($\tau = 1$) than smaller time ($\tau = 0.1$). Before discussing the influence of Q, it is to be noted that $Q > 0$ corresponds to the internal heat source and $Q < 0$ corresponds to heat sink. That is the way we have chosen the values of Q as $-2, -1, 0, 1, 2$. From Fig. 8, it is clear that, by increasing the values of $Q > 0$ the energy is released and these results in temperature increase, while, by increasing the values of $Q < 0$ energy is absorbed and this causes decrease in temperature field. Further, it is seen that, the temperature profile is higher in the presence of thermal radiation effect ($R = 5$) than its absence ($R = 0$). This is because, by introducing the thermal radiation provides more heat into the fluid, and as a result the temperature and the thickness of its boundary layer are intensified, which is similar result observed by Turkyilmazoglu and Pop [23]. From Fig. 9 it is observed that an increase in time parameter, results in a significant increase in the temperature profile. The similar trend is observed for the influence of thermal radiation parameter on the temperature profile as can be shown in Fig. 10. In addition, we observed in Fig. 10 that, the temperature of nanofluid is higher than that of ordinary fluid. The fluids with large Pr have low thermal diffusivity, so it causes low heat penetration. As a consequence, the temperature profile reduces significantly, which is illustrated as in Fig. 11.

The influence of chemical reaction, time and Schmidt number on dimensionless concentration profiles has been plotted in Figs. 12–14 correspondingly. Fig. 12 shows that, an increase in the chemical reaction parameter decreases the concentration profile rapidly. The central reason is that, the number of solute molecules undergoing chemical reaction gets increased as chemical reaction parameter increases, which leads to decrease in concentration field. Thus, a destructive chemical reaction reduces the solutal boundary layer thickness significantly. This outcome is in excellent agreement with that of obtained by Chamkha [14]. From Fig. 13, it is evident that the concentration of the fluid increases with increase in time. Fig. 14 anticipates that an increase in the Schmidt number corresponds to a weaker solute diffusivity which allows a shallower penetration of solutal effect. As a consequence the concentration decreases with increase in Sc. Thus, the solute boundary layer is thicker for smaller values of Sc and vice versa. We have chosen the Sc values as $Sc = 0.22,\ 0.30,\ 0.60,\ 0.78$ which correspond to hydrogen, helium, water vapor, and ammonia respectively. Further, it is observed that the concentration of profile becomes steeper in the presence of chemical reaction.

Fig. 15 is prepared to demonstrate the influence of heat source/sink on C_f and Nu versus ϕ. An increase in Q corresponds to increase in C_f whereas, opposite phenomenon can be seen with Nu. This is due to the fact that, for large values of heat source/sink parameter the momentum boundary layer thickens. Consequently, the skin friction co-efficient increases with heat source/sink parameter. The influence of thermal radiation and time parameter on C_f and Nu is quite same as the impact of Q, and this is as shown in Figs. 16 and 17. It is also observed from Figs. 15–17 that, both the skin friction co-efficient and Nusselt number decrease with increase in ϕ. Finally, Fig. 18 has been plotted to perceive the influence of time parameter on C_f and Sh versus K. The skin friction co-efficient and Nusselt number reveal an opposite behavior for the influence of both time and chemical reaction parameter. Table 2 explores that, the skin friction co-efficient is an increasing function of ϕ, Grt, Grc and τ, whereas it is decreasing function of M^2. It also depicts that, the drag force at the plate is lower when the plate is at stationary as compared with moving. Physically, the momentum boundary layer thickness is higher for large values of ϕ, Grt, Grc and τ. Hence, the skin friction drag is enhanced. The influence of Prandtl number on the Nu and C_f is qualitatively opposite, as can be seen in Table 3. Further, it is noted that the Nusselt number at the plate $\eta = 0$ is higher in the ordinary fluid than that of nanofluid.

4. Conclusion

An unsteady MHD free convection flow of a fluid past a vertical moving/stationary plate has been studied in the presence of nanoparticles, thermal radiation, heat source/sink and chemical reaction effects. The set of governing equations has been solved analytically using Laplace transform method. Based on the obtain results, the following conclusions are drawn;

- Intensifying magnetic field strength leads to reduction of drag force at the plate. On the other hand, the opposite trend is accounted as nanoparticle volume fraction varies.
- The effects of thermal radiation, heat source/sink and transient are qualitatively same on shear stress and Nusselt number.
- Larger values of the nanoparticle volume fraction showed a significant impact on velocity as well as temperature profile. By varying nanoparticle volume fraction, the flow and heat transfer characteristics could be controlled.
- The influence of thermal and solute Grashof number stabilizes the momentum boundary layer growth.
- As a result of thermal radiation and heat source/sink, the temperature profile enhances rapidly.
- The influence of Prandtl number and time parameter is opposite on temperature field.
- The presence of chemical reaction and heavier species reduces the concentration in the boundary layer.
- The inclusion of nanoparticles in the base fluids offers a potential in improving the heat transfer performance.

Acknowledgment

One of the authors (B.J. Gireesha) is thankful to the University Grants Commission, India, for the financial support under the scheme of Raman Fellowship for Indian Scholars in USA.

References

[1] W.F. Huges, F.J. Yong, The Electro-Magneto-Dynamics of Fluids, John Wiley and Sons, New York, USA, 1966.

[2] T. Sarpkaya, Flow of non-Newtonian fluids in a magnetic field, AIChE J. 7 (1961) 324–328.

[3] H.A. Attia, K.M. Ewis, Unsteady MHD Couette flow with heat transfer of a viscoelastic fluid under exponential decaying pressure gradient, Tamkang J. Sci. Eng. 13 (4) (2010) 359–364.

[4] M.E. Sayed-Ahmedand, H.A. Attia, MHD flow and heat transfer in a rectangular duct with temperature dependent viscosity and Hall effect, Int. Commun. Heat Mass Transfer 27 (8) (2000) 1177–1187.

[5] T. Hayat, O.U. Mehmood, Slip effects on MHD flow of third order fluid in a planar channel, Commun. Nonlinear Sci. Numer. Simul. 16 (3) (2011) 1363–1377.

[6] M. Modather, A.M. Rashad, A.J. Chamkha, Study of MHD heat and mass transfer oscillatory flow of a micropolar fluid over a vertical permeable plate in a porous medium, Turkis J. Eng. Environ. Sci. 33 (2009) 245–257.

[7] S. Nadeem, M. Hussain, M. Naz, MHD stagnation flow of a micropolar fluid through a porous medium, Int. J. Meccanica 45 (2010) 869–880.

[8] B.K. Jha, C.A. Apere, Unsteady MHD two-phase Couette flow of fluid-particle suspension, Appl. Math. Model. 37 (2013) 1920–1931.

[9] O.D. Makinde, T. Chinyoka, MHD Transient flows and heat transfer of dusty fluid in a channel with variable physical parameters and Navier slip boundary condition, Comput. Math. Appl. 60 (2010) 660–669.

[10] B.J. Gireesha, B. Mahanthesh, M.M. Rashidi, MHD boundary layer heat and mass transfer of a chemically reacting Casson fluid over a permeable stretching surface with non-uniform heat source/sink, Int. J. Ind. Math. 7 (2015) 14.

[11] B.J. Gireesha, B. Mahanthesh, P.T. Manjunatha, R.S.R. Gorla, Numerical solution for hydromagnetic boundary layer flow and heat transfer past a stretching surface embedded in non-Darcy porous medium with fluid-particle suspension, J. Nigerian Math. Soc. 34 (3) (2015) 267–285.

[12] B.J. Gireesha, B. Mahanthesh, R.S.R. Gorla, P.T. Manjunatha, Thermal radiation and Hall effects on boundary layer flow past a non-isothermal stretching surface embedded in porous medium with non-uniform heat source/sink and fluid-particle suspension, Heat Mass Transfer (2015) 1–15.

[13] D. Pal, B. Talukdar, Perturbation analysis of unsteady magnetohydrodynamic convective heat and mass transfer in a boundary layer slip flow past a vertical permeable plate with thermal radiation and chemical reaction, Commun. Nonlinear Sci. Numer. Simul. 15 (7) (2010) 1813–1830.

[14] A.J. Chamkha, MHD flow of a uniformly stretched vertical permeable surface in the presence of heat generation/absorption and a chemical reaction, Int. Commun. Heat Mass Transfer 30 (3) (2003) 413–422.

[15] I.J. Uwanta, E. Omokhuale, Viscoelastic fluid flow in a fixed plane with heat and mass transfer, Res. J. Math. Stat. 4 (3) (2012) 63–69.

[16] A.F. Khan, I. Samiulhaq, S. Shafie, Conjugate effects of heat and mass transfer on MHD free convection flow over an inclined plate embedded in a porous medium, PLoS ONE 8 (6) (2013) e65223, http://dx.doi.org/10.1371/journal.pone, 0065223.

[17] K. Das, S. Jana, P.K. Kundu, Unsteady MHD free convection flow near a moving vertical plate with ramped wall temperature, Int. J. Fluid Mech. Res. 41 (1) (2014).

[18] G.S. Seth, Md.S. Ansari, R. Nandkeolyar, MHD natural convection flow with radiative heat transfer past an impulsively moving plate with ramped wall temperature, Heat Mass Transfer 47 (2011) 551–561.

[19] K. Das, Effects of heat and mass transfer on MHD free convection flow near a moving vertical plate of a radiating and chemically reacting fluid, J. Sib. Fed. Univ. Math. Phys. 4 (2011) 18–31.

[20] R. Muthcuumaraswamy, G.K. Senthil, Heat and mass transfer effects on moving vertical plate in the presence of thermal radiation, Theor. Appl. Mach. (2004) 35–46.

[21] O.D. Makinde, Free convection flow with thermal radiation and mass transfer past a moving vertical porous plate, Int. Commun. Heat Mass Transfer 32 (2005) 1411–1419.

[22] B.J. Gireesha, B. Mahanthesh, Perturbation solution for radiating viscoelastic fluid flow and heat transfer with convective boundary condition in nonuniform channel with hall current and chemical reaction, ISRN Thermodyn. 2013 (2013) 1–14.
[23] M. Turkyilmazoglu, I. Pop, Soret and heat source effects on the unsteady radiative MHD free convection flow from an impulsively started infinite vertical plate, Int. J. Heat Mass Transfer 55 (2012) 7635–7644.
[24] M. Sheikholeslami, D.D. Ganji, Ferrofluid flow and heat transfer in a semi annulus enclosure in the presence of magnetic source considering thermal radiation, J. Taiwan Inst. Chem. Eng. 47 (2015) 6–17.
[25] S.U.S. Choi, D.A. Siginer, H.P. Wang, Enhancing Thermal Conductivity of Fluids with Nanoparticles, Developments and Applications of Non-Newtonian Flows, The American Society of Mechanical Engineers, New York, 1995, FED-vol. 231/MD-vol. 66, pp. 99–105.
[26] X. Wang, X. Xu, S.U.S. Choi, Thermal conductivity of nanoparticle fluid mixture, J. Thermophys. Heat Transfer 13 (1999) 474–480.
[27] J.A. Eastman, S.U.S. Choi, S. Li, W. Yu, L.J. Thompson, Anomalously increased effective thermal conductivity of ethylene glycol-based nanofluids containing copper nanoparticles, Appl. Phys. Lett. 78 (2001) 718–720.
[28] J. Buongiorno, Convective transport in nanofluids, ASME J. Heat Transfer 128 (2006) 240–250.
[29] M. Sheikholeslami, D.D. Ganji, Magnetohydrodynamic flow in a permeable channel filled with nanofluid, Sci. Iran 21 (1) (2014) 203–212.
[30] A.V. Kuznetsov, D.A. Nield, Natural convective boundary layer flow of a nanofluid past a vertical plate, Int. J. Therm. Sci. 49 (2010) 243–247.
[31] M.A.A. Hamad, I. Pop, Unsteady MHD free convection flow past a vertical permeable flat plate in a rotating frame of reference with constant heat source in a nanofluid, Heat Mass Transfer 47 (2011) 1517–1524.
[32] M. Turkyilmazoglu, Exact analytical solutions for heat and mass transfer of MHD slip flow in nanofluids, Chem. Eng. Sci. 84 (2014) 182–187.
[33] M. Turkyilmazoglu, I. Pop, Heat and mass transfer of unsteady natural convection flow of some nanofluids past a vertical infinite flat plate with radiation effect, Int. J. Heat Mass Transfer 59 (2013) 167–171.
[34] K. Das, Flow and heat transfer characteristics of nanofluids in a rotating frame, Alexandria Eng. J. 53 (3) (2014) 757–766.
[35] M. Sheikholeslami, D.D. Ganji, Unsteady nanofluid flow and heat transfer in presence of magnetic field considering thermal radiation, J. Braz. Soc. Mech. Sci. Eng. http://dx.doi.org/10.1007/s40430-014-0228-x.
[36] N. Freidoonimehr, B. Rostami, M.M. Rashidi, E. Momoniat, Analytical modelling of three-dimensional squeezing nanofluid flow in a rotating channel on a lower stretching porous wall, Math. Probl. Eng. 2014 (2014) 14 692728.
[37] B.J. Gireesha, B. Mahanthesh, R.S.R. Gorla, Suspended particle effect on nanofluid boundary layer flow past a stretching surface, J. Nanofluids 3 (3) (2014) 267–277.
[38] S. Das, R.N. Jana, O.D. Makinde, Mixed convective magnetohydrodynamic flow in a vertical channel filled with nanofluids, Eng. Sci. Technol. Int. J. 18 (2) (2015) 244–255.
[39] S. Das, R.N. Jana, Natural convective magneto-nanofluid flow and radiative heat transfer past a moving vertical plate, Alexandria Eng. J. 54 (2015) 55–64.
[40] B.J. Gireesha, B. Mahanthesh, I.S. Shivakumara, K.M. Eshwarappa, Melting heat transfer in boundary layer stagnation-point flow of nanofluid toward a stretching sheet with induced magnetic field, Eng. Sci. Technol. Int. J. (2015), http://dx.doi.org/10.1016/j.jestch.2015.07.012.
[41] M. Sheikholeslami, S. Soleimani, D.D. Ganji, Effect of electric field on hydrothermal behavior of nanofluid in a complex geometry, J. Mol. Liq. 213 (2016) 153–161.
[42] M. Sheikholeslami, M.M. Rashidi, D.D. Ganji, Numerical investigation of magnetic nanofluid forced convective heat transfer in existence of variable magnetic field using two phase model, J. Mol. Liq. 212 (2015) 117–126.
[43] M. Sheikholeslami, KKL correlation for simulation of nanofluid flow and heat transfer in a permeable channel, Phys. Lett. A 378 (45) (2014) 3331–3339.
[44] M. Sheikholeslami, D.D. Ganji, Ferrohydrodynamic and magnetohydrodynamic effects on ferrofluid flow and convective heat transfer, Energy 75 (2014) 400–410.